International Journal of Nanomedicine

Dovepress
Taylor & Francis Group

Open Access Full Text Article

ORIGINAL RESEARCH

Interleukin-2 Surface Displayed M1 Macrophage-Derived Extracellular Vesicles for Modulating the Tumor Microenvironment

Kyeong Tae Kim[1,*], Jeong Hyun Lee[1,*], Su Jin Kang[1], Won Jong Rhee[1–3]

[1]Department of Bioengineering and Nano-Bioengineering, Incheon National University, Incheon, 22012, Republic of Korea; [2]Division of Bioengineering, Incheon National University, Incheon, 22012, Republic of Korea; [3]Research Center for Bio Materials & Process Development, Incheon National University, Incheon, 22012, Republic of Korea

*These authors contributed equally to this work

Correspondence: Won Jong Rhee, Division of Bioengineering, Incheon National University, Incheon, 22012, Republic of Korea, Email wjrhee@inu.ac.kr

Purpose: Cancer immunotherapy aims to enhance the immune system's ability to recognize and eliminate cancer cells, providing a sustained and effective immune response. However, the tumor microenvironment (TME), characterized by an abundance of tumor-associated M2 macrophages and the presence of exhausted or naïve T cells (non-effector T cells), remains a major barrier to effective immunotherapy. Herein, inflammatory M1 macrophage-derived extracellular vesicles (M1EV) were surface-modified to display interleukin-2 (M1EV_IL2), aiming to develop a multifunctional cancer immunotherapeutic agent capable of modulating both innate and adaptive immune responses.

Methods: We engineered M1EV to label the surface with azide groups through metabolic glycoengineering and developed M1EV_IL2 that displayed IL-2 via bioorthogonal chemistry. M1EV_IL2 were purified by size-exclusion chromatography (SEC) and characterized through comprehensive analyses, including nanoparticle tracking analysis (NTA). In vitro macrophage repolarization and T cell activation were evaluated at the gene-expression level, followed by ex vivo assays assessing T-cell proliferation, cytokine secretion, and activation marker expression.

Results: M1EV_IL2 effectively retained the intrinsic physicochemical properties of EVs while displaying IL-2 stably on its surface. It upregulated M1 macrophage markers, IL-1β and CXCL10, while downregulating the M2 macrophage marker CD206, thereby inducing M2-to-M1 macrophage repolarization. In addition, M1EV_IL2 also activated $CD4^+$ T cells and induced the activation of naïve $CD8^+$ T cells to effector T cells, leading to enhanced cell proliferation and secretion of antitumor cytokines.

Conclusion: These results indicate that M1EV_IL2 has the potential to reshape the tumor immune landscape by simultaneously activating macrophages and T cells, thereby enhancing both innate and adaptive immune responses. Unlike conventional cancer therapies, which directly target tumor cells, M1EV_IL2 is expected to enhance immune responses, potentially mitigating adverse effects while improving therapeutic efficacy.

Keywords: cancer immunotherapy, extracellular vesicles, interleukin-2, macrophage repolarization, T cell activation

Introduction

Cancer is the second leading cause of death worldwide and is recognized as a major public health concern affecting approximately one in five individuals in the general population.[1,2] Conventional treatment modalities such as surgery, chemotherapy, hormone therapy, and radiation therapy have been applied for cancer treatment.[3] However, these approaches are associated with adverse effects, including treatment resistance, and damage to healthy organs and tissues.[4–6] Cancer immunotherapy has emerged as a promising therapeutic approach to enhance the immune system's ability to recognize and eliminate cancer cells, thereby improving antitumor immunity and clinical outcomes.[7] Notably, cancer immunotherapy using immune checkpoint inhibitors has been extensively studied and is currently employed in clinical practice as a cancer therapeutic strategy.[8,9] However, developing effective anticancer agents requires immune

Received: 12 June 2025
Accepted: 17 November 2025
Published: 26 November 2025

Graphical Abstract

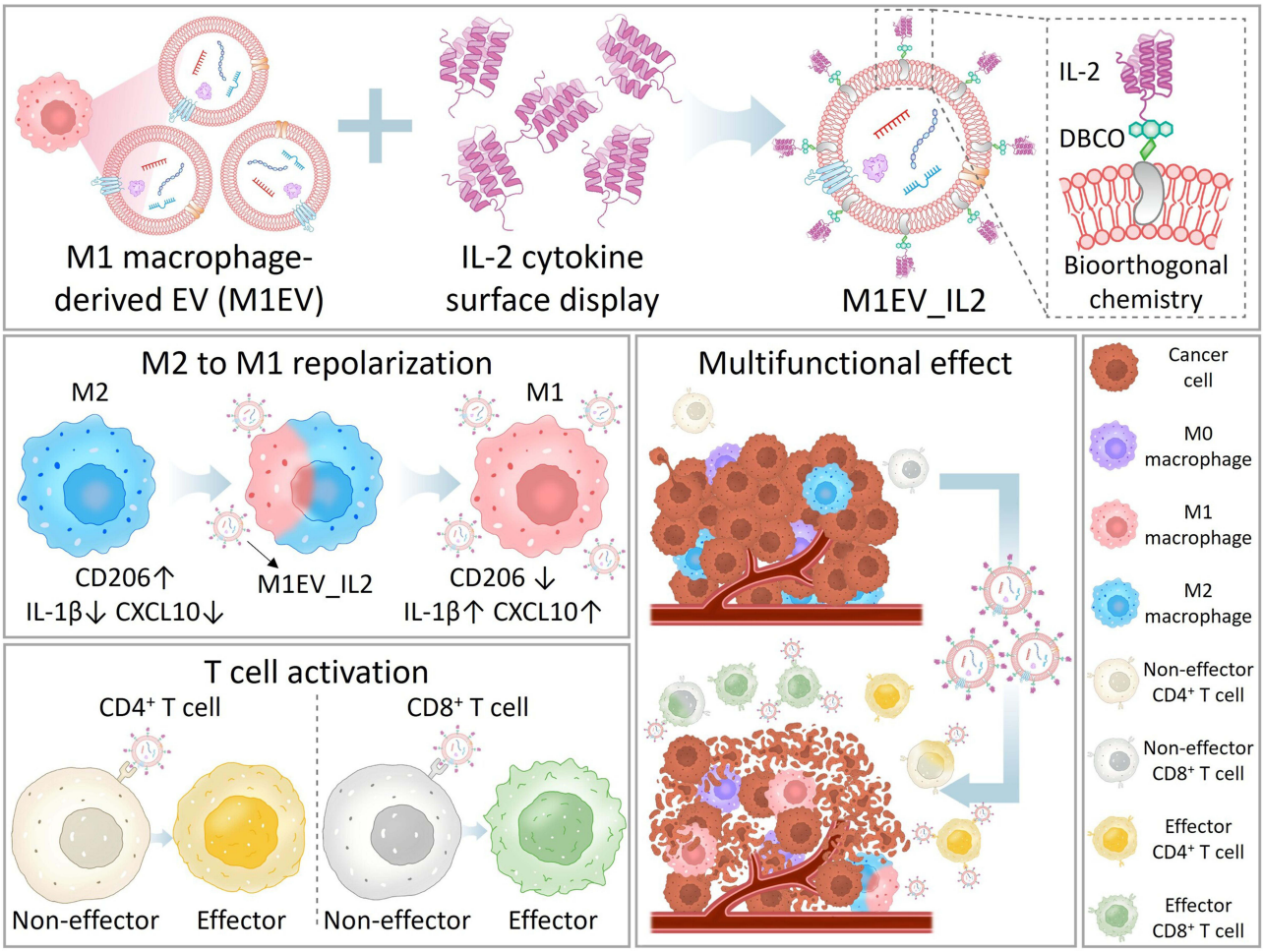

checkpoint inhibitors combined with novel therapeutic strategies, particularly those capable of modulating the tumor microenvironment (TME).[10,11]

The TME evolves in a complex and continuously adaptive process by promoting proliferation, apoptosis resistance, angiogenesis, invasion, metastasis, and immune evasion, thereby hindering the precise characterization of tumor immune cell composition.[12] Tumor-associated macrophages (TAMs) exhibiting M2-like properties are called anti-inflammatory macrophages and are abundant in the TME. These M2 macrophages significantly contribute to the establishment and modulation of the TME. They play a key role in wound healing. However, they predominantly exert immunosuppressive functions, facilitating tumor progression within the TME.[13–15] Conversely, M1 macrophages, known as pro-inflammatory macrophages, can directly eliminate or suppress tumor cells.[16] Unfortunately, the TME is typically dominated by M2 rather than M1 macrophages.[17] Furthermore, the activation of $CD8^+$ T cells, which destroy tumors via perforin and granzyme B, and $CD4^+$ T cells, which support $CD8^+$ T cell tumor-killing activity via interleukin-2 (IL-2) and interferon-gamma (IFN-γ), is crucial for successful cancer therapy.[18–20] However, T cells are often excluded from the tumor core or become functionally impaired due to the complex immune evasion mechanisms within the TME.[21,22] Consequently, non-activated T cells within the TME become exhausted or remain naïve, thereby failing to contribute to tumor elimination.[17,23] Therefore, developing a novel cancer therapeutic strategy capable of repolarizing M2 macrophages to M1 phenotype and activating T cells is essential to modulating the TME.

Extracellular vesicles (EVs) are nanosized vesicles, ranging from 30 to 1,000 nm in size, released from cells and enclosed by a lipid bilayer, including exosomes.[24–26] EVs carry various biomolecules, including proteins, mRNA, and miRNA, and are essential mediators of cell-to-cell communication via multiple complex mechanisms.[27–29] In particular, immune cell-derived EVs can induce macrophage repolarization via functional molecules such as miRNAs, thereby modulating their phenotype.[30–32] Furthermore, surface engineering strategies can be employed to enhance EV intrinsic functions and introduce additional functionalities.[33,34]

In this study, M1 macrophage-derived EVs (M1EV) was surface-modified and evaluated as a novel cancer immunotherapy approach, extending beyond in vitro models to ex vivo evaluation. Various EV engineering strategies have been investigated to overcome cancer. Unlike EV engineering approaches based on immune checkpoint inhibition,[35,36] our strategy directly activates T cells. Although IL-2 labeling on various EV surfaces has been explored to enhance antitumor efficacy,[37,38] the IL-2 surface-modified M1EV developed in this study are anticipated to serve as a novel multifunctional therapeutic agent, simultaneously augmenting both innate and adaptive immunity. M1EV induce tumor suppression by repolarizing abundant M2 macrophages within the TME to M1 macrophages. Additionally, IL-2, a T cell-activating cytokine, modified the M1EV surface to stimulate exhausted or naïve T cells, inducing to effector T cells. It activates $CD4^+$ T cells to support $CD8^+$ T cells and also directly activates $CD8^+$ T cells, enabling them to effectively eliminate tumor cells. The multifunctional IL-2-displaying M1 macrophage-derived EVs (M1EV_IL2) exhibit the potential to modulate both macrophages and T cells, thereby improving the TME by enhancing innate and adaptive immune responses. This strategy which stimulates and regulates immune responses rather than directly targeting cancer cells, may offer advantages in immune-based cancer treatment, including enhanced antitumor activity and sustained immunity.

Materials and Methods

Cell Culture

THP-1 and Jurkat cell lines were obtained from the Korean Cell Line Bank (Seoul, Korea) and maintained in the Roswell Park Memorial Institute Medium-1640 medium (RPMI-1640; Corning, VA, USA) supplemented with 10% (v/v) fetal bovine serum (FBS; Gibco, MA, USA) and 1% (v/v) penicillin-streptomycin (PS; Gibco, NY, USA). The cells were cultured at 37 °C in a 5% CO2 atmosphere.

Isolation of Naïve $CD8^+$ T Cells from Mouse Spleen

C57BL/6 male mice (11 weeks old) were obtained from DBL (Republic of Korea). Spleens of C57BL/6 were mechanically dissociated through a 70 μm Reversible strainer (Stem Cell Technologies, Canada) into cold PBS supplemented with 2% FBS and 10 mM EDTA. Red blood cells were removed using ACK lysis buffer (Gibco, NY, USA). Splenocytes were centrifuged at 300 × g for 5 min. Naïve $CD8^+$ T cells were isolated using the EasySep™ Mouse Naïve $CD8^+$ T Cell Isolation Kit (Stem Cell Technologies, Canada) via negative selection, according to the manufacturer's protocol. Naïve $CD8^+$ T cells were cultured at a density of 1×10^5 cells per well on 96 well plates pre- coated overnight with 1.0 μg/mL anti-CD3ε (Invitrogen, CA, USA) and 1.0 μg/mL anti-CD28 (Invitrogen, CA, USA), and maintained in the RPMI-1640 supplemented with 10% (v/v) FBS, 1% (v/v) PS, 0.05 mM β-mercaptoethanol (Sigma-Aldrich, MO, USA), 30 mM HEPES (Gibco, NY, USA), Gentamicin (1000×, Gibco, NY, USA), MEM Non-Essential Amino Acids Solution (100×, Gibco, NY, USA) and L-Glutamine (ATCC, VA, USA). The cells were cultured at 37 °C in a 5% CO2 atmosphere. All experiments were conducted in compliance with the regulations and ethical guidelines of the Incheon National University Animal Experiment Ethics Committee and were approved (INU-ANIM-2025-0016).

Preparation of DBCO-IL2 for Surface Engineering of M1EV

To synthesize dibenzocyclooctyne-interleukin-2 (DBCO-IL2), the EDC/NHS coupling reaction was performed in 0.1 M MES (Sigma-Aldrich, MO, USA) buffer at pH 6.0. The reaction proceeded with 25 μg/mL IL-2 (PeproTech, NJ, USA), 5 μg/mL DBCO-amine (BroadPharm, CA, USA), 2 mM 1-(3-Dimethylaminopropyl)-3-ethylcarbodiimide (EDC; Thermo Fisher Scientific, MA, USA) and 5 mM N-hydroxysulfosuccinimide sodium salt (Sulfo-NHS; Thermo Fisher

Scientific, NY, USA). EDC/NHS reaction was carried out at room temperature (RT) for 2 h under constant shaking in a final volume of 1 mL. Then, dialysis was performed for 3 days at 4 °C to remove unreacted residues.

Isolation of M1 Macrophage-Derived EVs (M1EV)

M1EV were isolated from THP-1 cells, which were cultured at a density of 4.0×10^5 cells/mL in RPMI-1640 supplemented with 200 ng/mL phorbol 12-myristate 13-acetate (PMA; Sigma-Aldrich, MO, USA) for 24 h. The medium was then replaced with PMA-free RPMI-1640 and incubated for an additional 24 h. Then, the medium was replaced with RPMI-1640 containing 1 μg/mL lipopolysaccharide (LPS; Sigma-Aldrich, MO, USA) and 20 ng/mL IFN-γ (PeproTech, NJ, USA), and the cells were cultured for another 48 h. To produce M1 macrophage-derived EVs, cells were incubated in a medium containing exosome-depleted FBS (Gibco, MA, USA). The supernatant culture media were centrifuged at 3,000 × g for 15 min at 4 °C to remove cells and cell debris. The resulting supernatant was concentrated using ultrafiltration (UF; 100K Amicon Ultra-15 filter unit; Millipore, MA, USA) by centrifugation at 5,000 × g. Finally, EVs were isolated from the concentrate using qEVoriginal Columns 70 nm (SEC columns; Izon Science, New Zealand) according to the manufacturer's instructions. Fraction 1 (F1) to 5 (F5) were collected at 500 μL each, and the remaining fractions were collected at 400 μL. EVs were finally harvested from Fraction 6 (F6) and Fraction 7 (F7).

Construction of M1EV_IL2

THP-1 cells were cultured at a density of 4.0×10^5 cells/mL in RPMI-1640 supplemented with 200 ng/mL PMA for 24 h. Subsequently, the medium was replaced, and the cells were incubated in a fresh medium containing 50 μM N-azidoacetylmannosamine-tetraacylated (Ac4ManNAz; MedChemExpress, NJ, USA) for 72 h. These metabolically glycoengineered cells were polarized to M1 macrophages by LPS and IFN-γ for 48 h in RPMI-1640 containing exosome-depleted FBS. The cell culture media were centrifuged at 3,000 × g for 15 min at 4 °C to remove cells and cell debris. Subsequently, the supernatant was incubated overnight with DBCO-IL2 under constant shaking at 4 °C. DBCO-IL2 was added at a concentration of 0.625 μg per 1 mL of supernatant. After incubation, M1EV_IL2 was isolated using UF and SEC. The EV fractions obtained by SEC were collected in the same manner as those of M1EV.

EV Characterization

The size distribution and concentration of M1EV and M1EV_IL2 were assessed using a Nanosight NS300 instrument (Malvern Instruments, UK). Transmission electron microscopy (TEM) imaging was conducted at the Electron Microscopy Facility, Eulji University. The protein concentration of all samples obtained after SEC was quantified using the Pierce™ BCA Protein Assay kit (Thermo Fisher Scientific, IL, USA). Zeta potential and polydispersity index (PDI) were measured at 25 °C using a Zetasizer Nano-ZS (Malvern Instruments, UK).

In vitro Investigation of Macrophage Repolarization from M2 to M1

To investigate the repolarization function of M1EV and M1EV_IL2 THP-1 cells were cultured at a density of 4.0×10^5 cells/mL in 6-well plates with RPMI-1640 supplemented with 200 ng/mL PMA for 24 h to differentiate into M0 macrophages. Subsequently, the cells were stimulated with 1 μg/mL LPS and 20 ng/mL IFN-γ or 20 ng/mL interleukin-4 (IL-4; PeproTech, NJ, USA) and 20 ng/mL interleukin-13 (IL-13; PeproTech, NJ, USA), followed by 24 h incubation to induce differentiation into M1 or M2 macrophages, respectively. To assess the M1EV_IL2 function, M2 macrophages were treated with M1EV or M1EV_IL2 for 24 h. Finally, macrophage polarization was evaluated at the gene-expression level using Quantitative real-time polymerase chain reaction (qRT-PCR).

In vitro Investigation of $CD4^+$ T Cell Activation

To evaluate the effect of surface-bound IL-2 on M1EV_IL2, CD4+ T cells, specifically Jurkat cells, were used. To activate Jurkat cells, the cells were cultured at a density of 3.0×10^5 cells/mL in RPMI-1640 medium, supplemented with 25 ng/mL PMA, 1 μM ionomycin (Sigma-Aldrich, MO, USA), and either M1EV or M1EV_IL2 for 24 h.

Ex vivo Investigation of $CD8^+$ T Cell Activation and Proliferation

As mentioned previously, naïve $CD8^+$ T cells were isolated from mouse spleens and cultured at a density of 1×10^5 cells per well in 96-well plates coated with anti-CD3ε and anti-CD28 with PBS or 10 ng/mL IL-2 or M1EV or M1EV_IL2 for 72 h. After incubation, the culture supernatant was centrifuged at 12,000 × g for 20 min using to remove debris, and then used for IFN-γ ezyme-linked immunosorbent assay (ELISA). Cell activation and proliferation were evaluated by water-soluble tetrazolium salt 1 (WST-1) and qRT-PCR analysis.

Western Blot Analysis

For Western blot analysis, M1EV and M1EV_IL2 were lysed in RIPA buffer. Primary antibodies against CD63 (MBL, Japan), CD81 (Abcam, UK), TSG101 (Abcam, UK), and GM130 (Abcam, UK) were used. Secondary antibodies included anti-mouse HRP (Abcam, UK) and anti-rabbit IgG conjugated to HRP (Cell Signaling Technology, MA, USA). Chemiluminescence was detected using the ECL Prime Western Blotting Detection Reagent (Cytiva, Italy), and images were captured using a ChemiDoc™XRS+ imaging system (Bio-Rad, USA).

ELISA

To detect and quantify IL-2 from M1EV_IL2, the ELISA MAX™ Deluxe Set for Human IL-2 (BioLegend, CA, USA) was used according to the manufacturer's instructions. Absorbance was measured at 450–570 nm using the Varioskan™ Flash Multimode Reader (Thermo Scientific, USA), and IL-2 concentrations were determined based on a standard curve. The amount of IFN-γ released from activated $CD8^+$ T cells was detected using the IFN-γ Mouse Uncoated ELISA Kit (Thermo Fisher Scientific, USA) according to the manufacturer's instructions and measured using the same reader.

qRT-PCR Analysis

The qRT-PCR was conducted to validate metabolic glycoengineering, macrophage polarization, and T-cell activation markers. RNA was isolated from cells using the FavorPrep™ Tri-RNA Reagent (FAVORGEN, Austria), following the manufacturer's instructions. The concentration and purity of the isolated RNA were determined using a microplate reader (BioTek Instruments, USA). cDNA was synthesized using the ReverTra Ace qPCR RT Master Mix (Toyobo, Japan). qRT-PCR was performed using the StepOnePlus Real-Time PCR System (Applied Biosystems, USA). Quantitative real-time PCR (qRT-PCR) data were analyzed using the comparative Ct ($2^{-\Delta\Delta Ct}$) method to determine relative gene expression. β-actin was used as a housekeeping gene to normalize gene expression. The primer sequences are listed in Table 1.

Table 1 Primer Sequences for qRT-PCR

Gene	Primer Sequence (5′ to 3′)			
	Forward	Tm (°C)	Reverse	Tm (°C)
Human β-actin	ATGAAGTGTGACGTTGACATCCG	58.2	GCTTGCTGATCCACATCTGCTG	60
Human IL-1β	AGCTGATGGCCCTAAACAGA	55.4	TCGGAGATTCGTAGCTGGAT	55.4
Human CXCL10	GAAAGCAGTTAGCAAGGAAAGGTC	58.4	ATGTAGGGAAGTGATGGGAGAGG	60.2
Human CD206	CATGGACAATGCGCGAG	54	ACCTGTGGCCCA AGACACGT	59.5
Human IL-2	AGAACTCAAACCTCTGGAGGAAG	58.2	GCTGTCTCATCAGCATATTCACAC	58.4
Human IFN-γ	CTGTTACTGCCAGGACCCAT	57.4	TCTGTCACTCTCCTCTTTCCAA	56.4
Mouse β-actin	CTGAGAGGGAAATCGTGCGT	57.4	CCACAGGATTCCATACCCAAGA	58.4
Mouse granzyme B	CTACTGCTGACCTTGTCTCT	55.4	AAAGTAAGGCCATGTAGGGT	53.4
Mouse IFN-γ	GACAATGAACGCTACACACT	53.4	TAGGCTTTCAATGACTGTGC	53.4
Mouse TNF-α	CTGTGAAGGGAATGGGTGTT	55.4	GGTCACTGTCCCAGCATCTT	57.4

https://doi.org/10.2147/IJN.S546777

WST-1 Assay

The proliferative effects of M1EV and M1EV-IL2 were analyzed using the EZ-Cytox kit (DoGenBio, Korea) following the manufacturer's instructions. Absorbance values at 450 nm were measured using the Varioskan™ Flash Multimode at 0 h for naïve $CD8^+$ T cells and 72 h for inducer-treated $CD8^+$ T cells. Cell proliferation was determined as a percentage based on the formula (Abscorbance of inducer-treated $CD8^+$ T at 72 h /Abscorbance of naïve $CD8^+$ T cells at 0 h) × 100.

Statistical Analysis

Statistical analyses were conducted using one-way and two-way analysis of variance (ANOVA), *t*-test followed by a multiple comparison test using GraphPad Prism 8.4.2 software (GraphPad, CA, USA). Statistical significance was defined as $*p < 0.05$, $**p < 0.01$, and $***p < 0.001$; NS, not significant ($p > 0.05$). Data are expressed as mean ± standard deviation (SD), $n \geq 3$ independent biological replicates. The graphical Abstract, schematic figures, and hand-drawn illustrations of biomolecules, cells, and vesicles, and related elements were created using Procreate (Savage Interactive Pty Ltd., Australia), Adobe Illustrator (Adobe Inc., CA, USA), and Microsoft PowerPoint (Microsoft Corp., WA, USA).

Results and Discussion

Surface Engineering of M1EV via Metabolic Glycoengineering and Bioorthogonal Chemistry for IL-2 Conjugation

M1EV, containing biomolecules such as proteins and miRNAs, can induce M2 macrophage repolarization to M1 macrophages.[39–42] Additional surface modifications are required to enhance this repolarization and confer additional functionality. Metabolic glycoengineering, a widely recognized strategy, enables specific surface conjugation via bioorthogonal chemistry by introducing azide groups the cell surface.[43,44] Herein, metabolic glycoengineering, a bioorthogonal chemistry method, facilitated surface modification, offering high biocompatibility and rapid conjugation efficiency.[45–48]

To achieve this, THP-1 monocytes were differentiated into M1 macrophages while expressing azide groups on their surface (Figure 1A). THP-1 cells require initial polarization to M0 macrophages, which can subsequently differentiate into either M1 or M2 macrophages.[49] This initial polarization was achieved by stimulating THP-1 cells with PMA, thereby inducing their differentiation to M0 macrophages.[50] Azide groups were introduced onto the surface of these M0 macrophages via Ac4ManNAz treatment, followed by differentiation into M1 macrophages via co-treatment with LPS and IFN-γ.

A comparative analysis was conducted via qRT-PCR analysis to investigate whether Ac4ManNAz-treated M1 macrophages retain the M1 macrophage functions (Figure 1B). M0 macrophages, treated only with PMA, were designated as the control group and were compared to the M1 macrophages treated with the inducers, LPS and IFN-γ, but without Ac4ManNAz. qRT-PCR analysis of the M1 marker interleukin-1 beta (IL-1β) showed significantly elevated expression in M1 macrophages, and Ac4ManNAz-treated M1 macrophages compared to M0 macrophages, with a 7.4 ± 1.6-fold and a 7.0 ± 3.5-fold increases, respectively. No significant difference in IL-1β expression was observed between M1 macrophages and Ac4ManNAz-treated M1 macrophages. Additionally, the distinct morphological differences between M0 and M1 macrophages, readily detected under a microscope,[51] were assessed. As shown in Supplemental Figure 1, both M1 and Ac4ManNAz-treated M1 macrophages exhibited similar elongated morphologies distinct from M0 macrophages. These results suggest that Ac4ManNAz-treated M1 macrophages successfully differentiated into M1 macrophages, maintaining characteristic M1 macrophage functions and indicating their potential to secrete M1EV.

Ac4ManNAz-treated M1 macrophages, characterized by azide group expression on their surface, facilitate DBCO conjugation, enabling the potential to confer additional functions. This indicates that, unlike standard M1 macrophages, DBCO-molecule conjugation is feasible (Figure 1C). To confirm successful bioorthogonal chemistry on the cell surface, Ac4ManNAz-treated M1 macrophages, with surface azide groups, were incubated with DBCO-Cy5 (Figure 1D). Fluorescence microscopy imaging confirmed DBCO conjugation to Ac4ManNAz-treated M1 macrophages via bioorthogonal chemistry. M1 macrophages without azide expression exhibited weak fluorescence with DBCO-Cy5, whereas Ac4ManNAz-treated M1 macrophages expressing azide groups showed strong fluorescence signals with DBCO-Cy5.

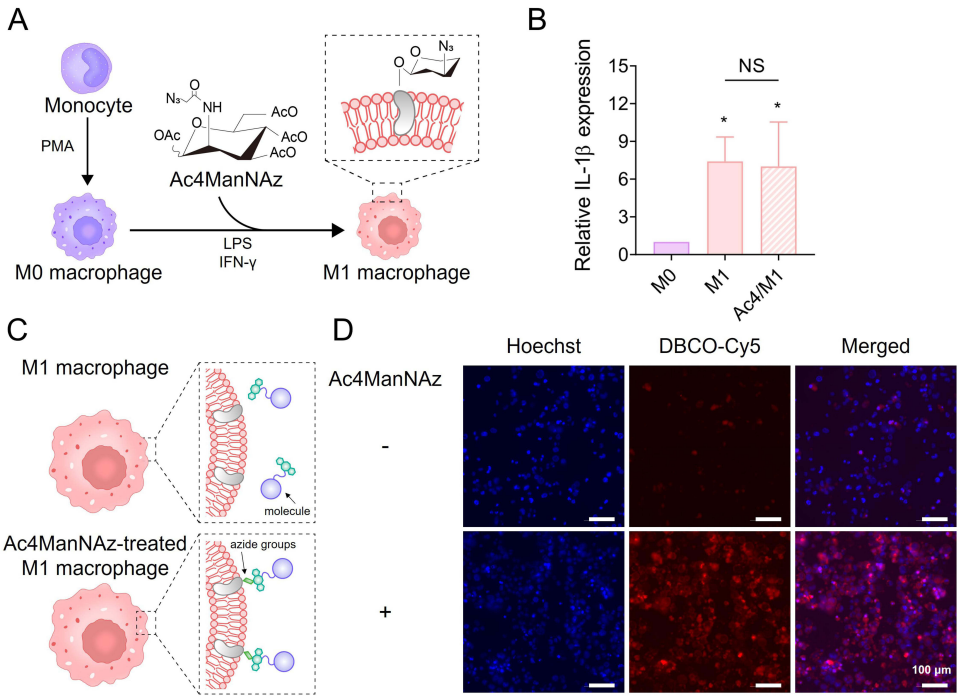

Figure 1 Metabolic glycoengineering and bioorthogonal chemistry for surface modification of M1EV. (**A**) Schematic representation of M1 macrophage polarization and metabolic glycoengineering, illustrating the differentiation of monocytes into M0 macrophages using PMA and their subsequent polarization into M1 macrophages with IFN-γ and LPS. This also depicts introducing azide groups onto the M1 macrophage surface through Ac4ManNAz treatment to facilitate bioorthogonal chemistry with DBCO-functionalized molecules. (**B**) qRT-PCR analysis comparing the relative expression level of IL-1β between M1 macrophages and Ac4ManNAz-treated M1 macrophages (Ac4/M1). (**C**) Schematic comparison of cell surfaces between M1 macrophages and Ac4ManNAz-treated M1 macrophages. Introduction of azide groups (green) onto the surface of Ac4ManNAz-treated M1 macrophages via metabolic glycoengineering, enabling bio-orthogonal conjugation with DBCO-functionalized molecules. (**D**) Fluorescence microscopy imaging of macrophages labeled with DBCO-Cy5 after Ac4ManNAz treatment. Hoechst staining shows nuclei (blue), while DBCO-Cy5 indicates successful surface labeling (red). The merged image highlights specific azide-dependent bioorthogonal chemistry, with scale bars representing 100 μm. The data are presented as mean ± SD, n ≥ 3. (*p < 0.05).
Abbreviation: NS, not significant.

These results validate the successful expression of azide groups on Ac4ManNAz-treated M1 macrophages, demonstrating their capability to facilitate DBCO conjugation on the cell surface.

Purification of M1EV Produced from M1 Macrophages

First, M1EV produced from M1 macrophages were purified and analyzed (Figure 2A). The M1 macrophage culture medium was centrifuged to remove cells and cell debris, followed by UF. Subsequently, M1EV were purified and isolated using SEC, followed by characterization of their size distribution and protein concentration through NTA and BCA assay, respectively. The BCA assay was quantitatively evaluated based on a standard curve with an R^2 value of 0.9961 (Supplemental Figure 2). M1EV were separated into 33 fractions using SEC, with the majority observed in fractions 6, 7, and 8 (Figure 2A). As the fraction number increased, protein concentration increased, confirming the successful separation of M1EV from protein impurities derived from the cell culture medium. To select the main fraction for the experiment, the size distribution and particle count of EV-containing fractions were analyzed via NTA (Figure 2B). Accordingly, fraction 6 and 7, exhibiting the highest yield and falling within the typical EV size range, were selected and designated M1EV (Supplemental Figure 3A).

Generation of M1EV_IL2 via Metabolic Glycoengineering

Similar production processes were adopted to construct and purify M1EV_IL2 (Figure 2C–E). Since Ac4ManNAz-treated M1 macrophages exhibited azide group expression on their surface, it is anticipated that EVs produced from these macrophages would also display azide groups on their surface. To impart immunomodulatory properties and construct M1EV_IL2, IL-2 was conjugated to the surface of M1EV derived from Ac4ManNAz-treated M1 macrophages in the

https://doi.org/10.2147/IJN.S546777

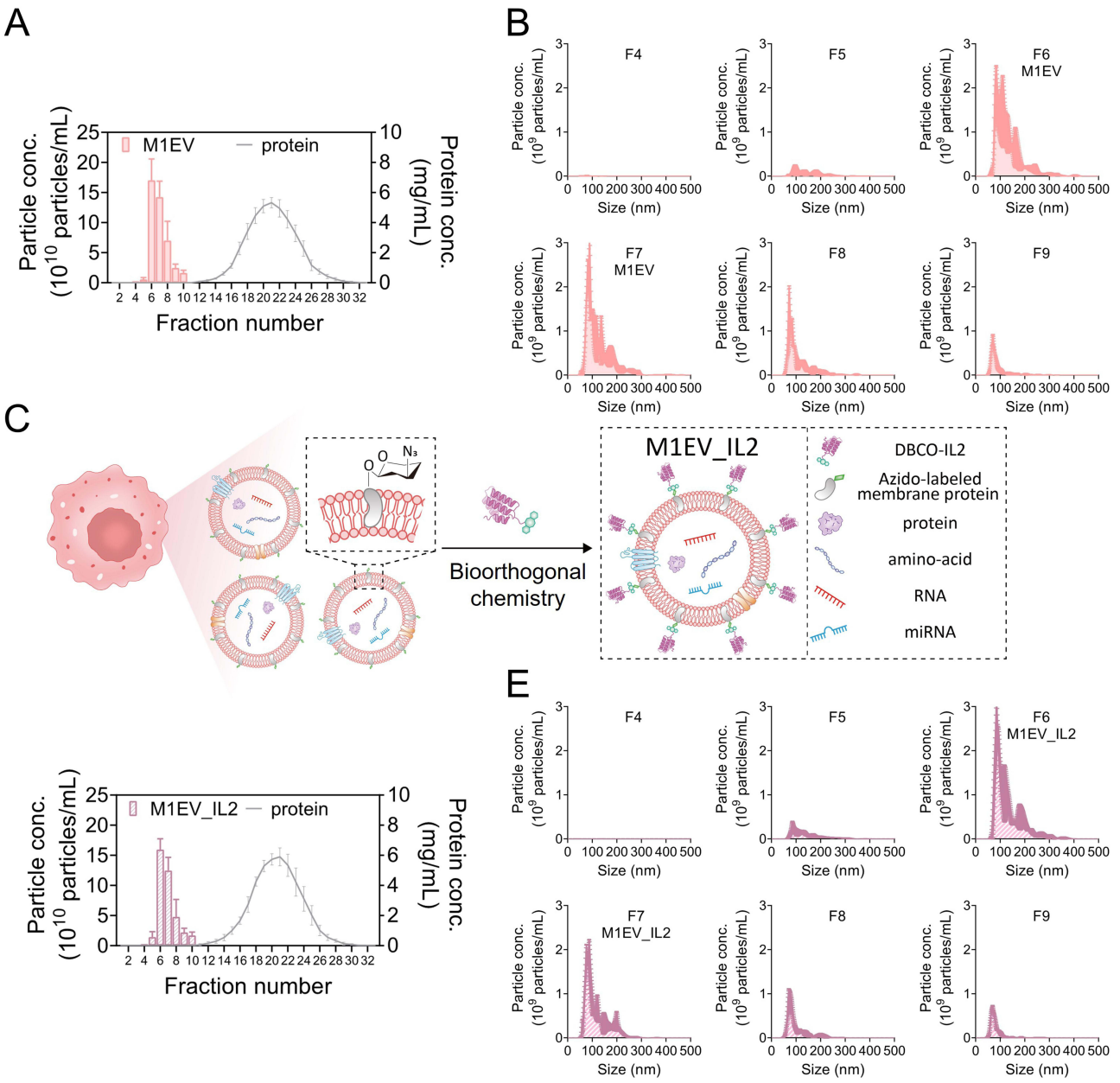

Figure 2 Evaluation of M1EV and M1EV_IL2. (**A**) SEC-based fractionation of M1EV showing particle concentration (pink bars) and protein concentration (gray line) in each fraction. (**B**) NTA-based analysis of M1EV, including size distribution and particle count across various SEC fractions 4–9 (F4-9). (**C**) Schematic representation of M1EV_IL2 engineering via bioorthogonal chemistry between Ac4ManNAz-treated M1 macrophage-derived EVs and DBCO-IL2. (**D**) SEC-based fractionation of M1EV_IL2 showing particle concentration (hatched plum bars) and protein concentration (gray line) in each fraction. (**E**) NTA-based analysis of M1EV_IL2, including size distribution and particle count across various SEC F4-9. The data are presented as mean ± SD, n ≥ 3.

culture medium via bioorthogonal chemistry (Figure 2C). Subsequently, EVs were purified and separated using the same method used for M1EV production. As shown in Figure 2D, EVs conjugated with IL-2 were successfully purified and separated from protein impurities. NTA was performed to analyze the size distribution and particle count as for M1EV (Figure 2E). Fractions 6and 7, exhibiting the highest yield and falling within the typical EV size range, were designated as M1EV_IL2 hereafter (Supplemental Figure 3B).

Physicochemical and Functional Properties of M1EV_IL2 Compared with M1EV

EVs possess inherent characteristics, including size, PDI, zeta potential, and morphology. To examine the chemical, physical, and biological properties of the produced EVs, M1EV and M1EV_IL2 were characterized. Maintaining

consistent EV characteristics is critical when surface modification is introduced. Therefore, NTA and Zetasizer were used to analyze the concentration, size distribution, and physicochemical properties accurately. Initially, the size distributions of M1EV and M1EV_IL2 were directly compared, revealing no noticeable difference (Figure 3A). The EV concentration was $1.6 \pm 0.5\times10^{11}$ and $1.5 \pm 0.4\times10^{11}$ particles/mL for M1EV and M1EV_IL2, respectively (Figure 3B). When converted to the total particle count per 1 mL of culture medium, M1EV contained $1.6 \pm 0.5\times10^{9}$ particles, while M1EV_IL2 contained $1.5 \pm 0.4\times10^{9}$ particles, indicating no significant difference. And M1EV and M1EV_IL2 achieved yields of $2.9 \pm 0.6\times10^{9}$ particles per 1 mL and $2.0 \pm 0.7\times10^{9}$ particles per 1 mL of culture medium (Figure 3C). This indicates that neither Ac4ManNAz treatment nor IL-2 display resulted in a significant reduction or loss of EVs, ensuring the scalability of M1EV_IL2 production.

The average sizes of M1EV and M1EV_IL2 were 130.5 ± 1.7 and 126.4 ± 4.6 nm, respectively, showing no significant difference between the EVs (Figure 3D). This indicates that displaying IL-2 on the EV surface did not introduce structural alterations in the EVs during surface modification. The PDI values were measured, revealing a PDI value of 0.2837 ± 0.981 for M1EV, and 0.3387 ± 0.0452 for M1EV_IL2, with no significant differences observed between the two groups (Figure 3E). Furthermore, the zeta potential was measured at −19.0 ± 3.2 mV for M1EV and −14.0 ± 9.0 mV for M1EV_IL2, again indicating no significant differences (Figure 3F). Western blot analysis was performed to verify the presence of representative positive and negative EV markers in both M1EV and M1EV_IL2 (Figure 3G). TEM imaging confirmed that both M1EV and M1EV_IL2 exhibited identical EV morphology consistent with the characteristic cup-shaped structure observed in EVs (Figure 3H).[52] Both M1EV and M1EV_IL2 maintained

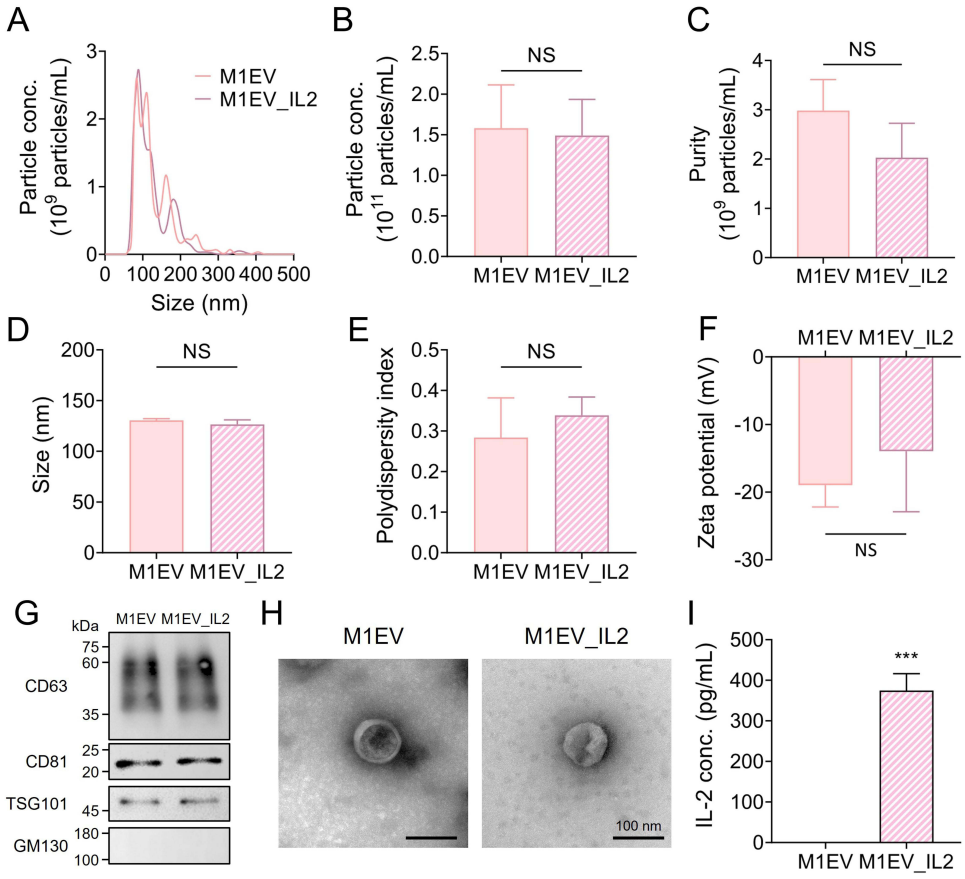

Figure 3 Comparative functional analysis of M1EV and M1EV_IL2. (**A**) NTA-based size distribution analysis of M1EV and M1EV_IL2. (**B**) Measurement of EV concentration in M1EV and M1EV_IL2. (**C**) EV yield per 1 mL of culture medium for M1EV and M1EV_IL2 based on the main fraction (F6, F7). (**D**) Size analysis of M1EV and M1EV_IL2. (**E**) PDI analysis of M1EV and M1EV_IL2. (**F**) Zeta potential evaluation of M1EV and M1EV_IL2. (**G**) Western blot assay. CD63, CD81, and TSG101 were evaluated as positive EV markers, while GM130 was assessed as a negative EV marker. (**H**) TEM-based morphological characterization of M1EV and M1EV_IL2. Scale bar = 100 nm. (**I**) ELISA-based analysis for IL-2 quantification in M1EV and M1EV_IL2. The data are presented as mean ± SD, n ≥ 3. (***p < 0.001).
Abbreviation: NS, not significant.

https://doi.org/10.2147/IJN.S546777

stable size and concentration for up to two weeks under 4 °C and 10% FBS conditions (Supplemental Figure 4A and 4B). Furthermore, under 37 °C and 10% FBS conditions, a decrease in concentration was observed after day 12, indicating that M1EV_IL2 is suitable for maintaining stability and functionality in physiological environments (Supplemental Figure 4C and 4D). To demonstrate the IL-2 conjugation in M1EV_IL2, ELISA was performed to quantify IL-2 levels in M1EV and M1EV_IL2. During EV isolation, free DBCO-IL2 was removed via UF, as confirmed by ELISA (Supplemental Figure 5A). These results indicate that free DBCO-IL2 was eliminated through UF and subsequent SEC purification, and only IL-2 conjugated to M1EV_IL2 was quantified. Upon using equal numbers of EVs for IL-2 measurement, a negligible concentration of IL-2 was observed in M1EV, whereas 374.7 ± 41.7 pg/mL was measured for M1EV_IL2 (Figure 3I). In addition, isolated M1EV_IL2 maintained over 90% efficiency even after 4 days at 2–8 °C, indicating high stability (Supplemental Figure 5B). This clearly indicates that IL-2 was successfully conjugated on the surface of M1EV_IL2 without altering the M1EV physical properties.

In vitro Investigation of Macrophage Repolarization from M2 to M1 Using M1EV_IL2

M2 macrophages are more abundant than M1 macrophages in the TME and promote proliferation, apoptosis resistance, and angiogenesis.[12] Consequently, repolarizing macrophages from M2 to M1 is essential for inducing an anti-tumor response within the TME. EVs produced from M1 macrophages contain functional molecules, including miRNAs, involved in M2 macrophage repolarization to M1 macrophages, contributing to tumor suppression.[30,53,54] Accordingly, the M1EV_IL2 ability to repolarize M2 macrophages to M1 macrophages was evaluated, considering its retention of M1EV functional properties.

To investigate the repolarization function of M1EV and M1EV_IL2, THP-1–derived macrophages were successfully differentiated to M0, M1, and M2 macrophages through sequential stimulation with PMA, LPS/IFN-γ, or IL-4/IL-13 (Figure 4A), and repolarization to M1 macrophages was evaluated using qRT-PCR (Figure 4B–D). IL-1β and C-X-C motif chemokine ligand 10 (CXCL10) were used as representative M1 macrophage markers,[50,55] whereas CD206 served as a representative M2 macrophage marker.[56] Results showed that the IL-1β relative expression increased 7.14 ± 1.3-fold in M1 macrophages compared to that in M0 macrophages, whereas no significant difference was observed

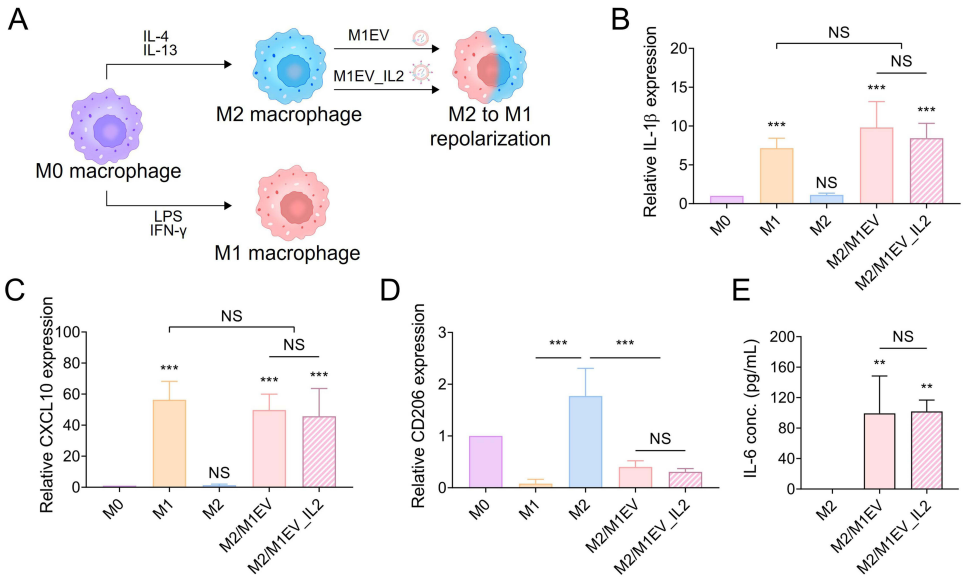

Figure 4 Evaluation of M1EV_IL2 repolarization ability from M2 macrophages to M1 macrophages. (**A**) Schematic illustration of M1 macrophages polarization and M2 to M1 repolarization, depicting monocyte differentiation into M0 macrophages using PMA, polarization into M1 or M2 macrophages with IFN-γ/LPS or IL-4/IL-13, respectively, and subsequent treatment of M2 macrophages with M1EV or M1EV_IL2 for M1 repolarization assessment. IL-1β and CXCL10 are used as M1 macrophage markers, and CD206 is used as an M2 macrophage marker. (**B**) qRT-PCR analysis of IL-1β expression in M2 macrophages treated with M1EV or M1EV_IL2 as an M1 macrophage marker. (**C**) qRT-PCR analysis of CXCL10 expression in M2 macrophages treated with M1EV or M1EV_IL2 as an M1 macrophage marker. (**D**) qRT-PCR analysis of CD206 expression in M2 macrophages treated with M1EV or M1EV_IL2 as an M2 macrophage marker. The data are presented as mean ± SD, n ≥ 3. (***p < 0.001; NS: not significant). (**E**) ELISA-based measurement of IL-6 secretion to evaluate the M2 to M1 repolarization of M1EV and M1EV_IL2. The data are presented as mean ± SD, n ≥ 3. (**p < 0.01).
Abbreviation: NS, not significant.

in the case of M2 macrophages (Figure 4B). Furthermore, when M2 macrophages were treated with M1EV or M1EV_IL2, the IL-1β expression level increased 9.81 ± 3.3-fold and 8.43 ± 1.9-fold, respectively, compared to that in M0 macrophages, and no significant difference in IL-1β expression was observed between the two treatment groups. Similarly, the CXCL10 gene expression level, another M1 macrophage marker, increased 56.3 ± 11.9-fold in M1 macrophages compared to that in M0 macrophages (Figure 4C). The CXCL10 expression level in M2 macrophages treated with M1EV or M1EV_IL2 increased 49.7 ± 10.3-fold and 45.7 ± 17.9-fold, respectively, compared to that in M0 macrophages, and no significant difference was observed in CXCL10 expression between M2 macrophages supplemented with M1EV or M1EV_IL2. This indicates M1EV and M1EV_IL2 promoted pro-inflammatory gene expression, including IL-1β and CXCL10, thereby exerting anti-tumor effects through inflammatory responses. Additionally, the CD206 gene expression level, a representative M2 macrophage marker, was evaluated (Figure 4D), and it increased 1.7 ± 0.5-fold in M2 macrophages and decreased approximately 12.6-fold in M1 macrophages, compared to that in M0 macrophages. In M2 macrophages supplemented with M1EV or M1EV_IL2, CD206 expression decreased approximately 2.5-fold and 3.2-fold, respectively, compared to that in M0 macrophages. Compared to the CD206 expression level in normal M2 macrophages, this represents approximately 4.2-fold and 5.6-fold reduction, respectively. These results indicate that both M1EV and M1EV_IL2 significantly reduced the level of M2 macrophages while increasing M1 macrophages. Additionally, Ac4ManNAz-treated M1EV (Ac4M1EV) induced the repolarization of M2 macrophages into M1 macrophages, similar to M1EV, indicating that the introduction of azide groups on the surface did not affect its intrinsic function (Supplemental Figure 6). Furthermore, IL-6 cytokine secretion from M1 macrophages was evaluated (Figure 4E). M2 macrophages treated with M1EV or M1EV_IL2 were repolarized into the M1 phenotype, secreting specific cytokines, indicating that M1EV_IL2 can promote functional cytokine production in addition to gene-level regulation. This confirms that M1EV_IL2 retains the inherent M1EV repolarization function, promoting the M2 macrophage repolarization into M1 macrophages. Consequently, this suggests its potential to shift the M2 macrophage-dominant TME to an M1 macrophage-enriched environment.

In vitro Investigation of $CD4^+$ T Cell Activation Using M1EV_IL2

Unlike macrophages, which are involved in innate immune responses, T cells are essential for adaptive immune responses.[57] T cells within the TME are often exhausted or naïve, rendering their activation crucial for antitumor immunity.[23] IL-2 plays a critical role in activating exhausted or naïve T cells, thereby contributing to the improvement of the tumor immune microenvironment.[58–60] $CD4^+$ T cells, also known as helper T cells, regulate and activate immune cells by secreting various cytokines.[61] Through distinct subsets such as T helper 1 (Th1) and Th2 cells, they play a significant role in regulating immune responses.[62] Since CD4+ T cells express CD25, an IL-2 receptor, on their surface, they can induce slight activation through downstream signaling pathways such as JAK/STAT5.[63,64] Therefore, a slight upregulation of activation-related cytokines such as IL-2 and IFN-γ may occur.[65] To evaluate the effect of surface-bound IL-2 on T cell activation, $CD4^+$ T cells (Jurkat cells) were stimulated with PMA and ionomycin for 24 h in the presence of M1EV or M1EV_IL2. After incubation, qRT-PCR was performed to evaluate the gene expression levels of $CD4^+$ T cell activation markers, IL-2 and IFN-γ (Figure 5A). Compared to stimulation with PMA and ionomycin alone (control), $CD4^+$ T cells supplemented with M1EV showed only a 1.1 ± 0.3-fold increase in IFN-γ expression level, whereas those supplemented with M1EV_IL2 exhibited a 1.5 ± 0.2-fold increase (Figure 5B). Statistical analysis revealed no significant difference between the M1EV and the control groups, whereas the M1EV_IL2 exhibited a slight but noticeable difference. Moreover, the IL-2 expression level increased 0.8 ± 0.2-fold in the M1EV group compared to that in the control group, showing no significant difference. However, M1EV_IL2 supplementation resulted in a 1.8 ± 0.2-fold increase, indicating IL-2 expression upregulation (Figure 5C). This suggests that $CD4^+$ T cells are stimulated by IL-2 displayed on the surface of M1EV_IL2. This demonstrates that, compared to M1EV, M1EV_IL2 possesses a role in $CD4^+$ T cell activation.

Ex vivo Investigation of $CD8^+$ T Cell Activation and Proliferation Using M1EV_IL2

$CD8^+$ T cells, also known as cytotoxic T cells, mediate immune responses by directly eliminating cancer cells through factors such as granzyme B and perforin.[66,67] Furthermore, $CD8^+$ T cells possess a higher abundance of IL-2 receptors

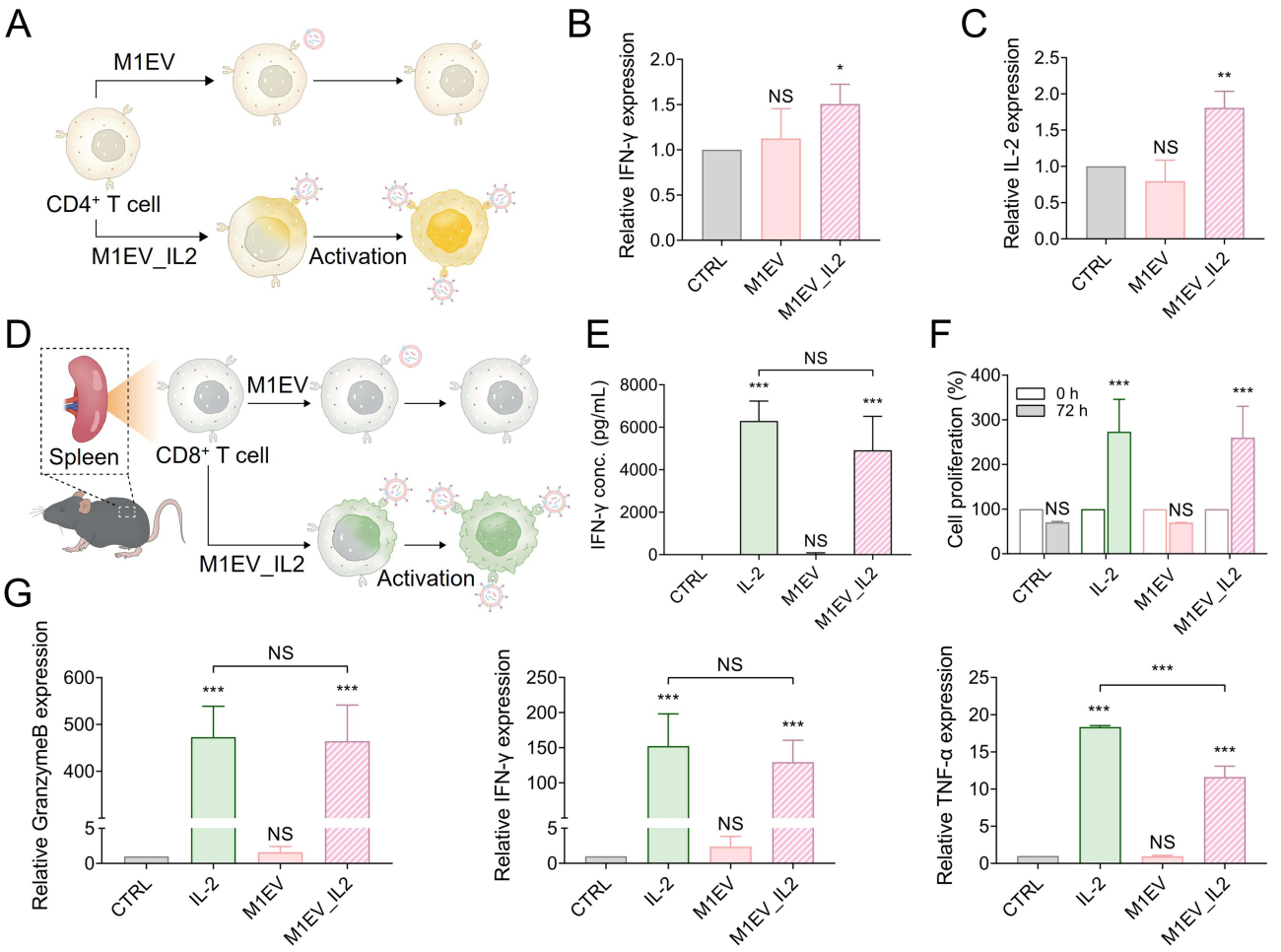

Figure 5 M1EV_IL2-induced activation of $CD4^+$ and $CD8^+$ T cells. (**A**) Schematic illustration of $CD4^+$ T cell activation by M1EV and M1EV_IL2, depicting $CD4^+$ T cell stimulation with M1EV or M1EV_IL2 and subsequent activation assessment based on IFN-γ and IL-2 expression. (**B** and **C**) Definition of the CTRL group as the condition treated with PBS. qRT-PCR analysis of IFN-γ, IL-2 expression in $CD4^+$ T cells treated with M1EV or M1EV_IL2. (**D**) Schematic illustration of $CD8^+$ T cell activation induced by M1EV or M1EV_IL2, including isolation of naïve $CD8^+$ T cells from mouse spleens followed by treatment with M1EV or M1EV_IL2 to evaluate proliferation and activation. (**E–I**) Definition of the CTRL group (negative control) as the cells treated with PBS, and the IL-2 group (positive control) as the condition treated with 10 ng/mL IL-2, followed by analysis 72 hours post-treatment with each inducer. (**E**) ELISA-based analysis of IFN-γ levels in the culture supernatant of $CD8^+$ T cells. (**F**) $CD8^+$ T cell proliferation via WST-1 assay. (**G–I**) qRT-PCR analysis of granzyme B, IFN-γ, and TNF-α expression in $CD8^+$ T cells treated with M1EV or M1EV_IL2. The data are presented as mean ± SD, n ≥ 3. (*$p < 0.05$; **$p < 0.01$; ***$p < 0.001$).

Abbreviation: NS, not significant.

compared to $CD4^+$ T cells, enabling more efficient activation.[68] Considering the importance of $CD8^+$ T cells in directly targeting cancer cells, assessing their activation is crucial. To examine the effect of M1EV_IL2 on $CD8^+$ T cell activation, naïve $CD8^+$ T cells were isolated from mouse spleens (Figure 5D). A negative control (CTRL) was established by treating cells with phosphate-buffered saline (PBS), while a positive control (IL-2) was set up by treating cells with 10 ng/mL IL-2. After 72 h, ELISA was performed on the culture supernatant to analyze IFN-γ secretion, a characteristic marker of $CD8^+$ T cell activation (Figure 5E). IFN-γ was not detected in the CTRL group, whereas the IL-2 group exhibited an IFN-γ level of 6,299 ± 932 pg/mL. Notably, a high level of IFN-γ was detected when naïve $CD8^+$ T cells were supplemented with M1EV_IL2, whereas a negligible level was detected in M1EV-supplemented cells. The IFN-γ levels were 25.3 ± 60.46 and 4,917 ± 1,599 pg/mL in cells supplemented with M1EV and M1EV_IL2, respectively. Furthermore, cytokine secretion from naïve $CD8^+$ T cells was induced in an M1EV_IL2 dose-dependent manner (Supplemental Figure 7).

To assess the M1EV_IL2 effect on $CD8^+$ T cell proliferation, a WST-1 assay was performed (Figure 5F). In the CTRL group, relative cell concentration decreased to 70.5 ± 1.8%, showing no significant difference from that in the M1EV group (69.7 ± 0.3%). This indicates that naïve $CD8^+$ T cells were not activated. Conversely, both the IL-2 group and

M1EV_IL2 supplemented cells exhibited relative concentration increases of 273.3 ± 72.55% and 259.8 ± 70.22%, respectively. Additionally, differences in cell phenotype were observed (Supplemental Figure 8). Initially, cultured naïve $CD8^+$ T cells (0 h) appeared small and floating. However, after 72 h, cells in the CTRL and M1EV supplemented groups, which were not IL-2-stimulated, showed no significant changes or appeared dark under the microscope, indicating cell death. Conversely, cells in the IL-2 and M1EV_IL2-supplemented groups exhibited increased cell size and proliferation, confirming the stimulatory effect of IL-2 on the surface of M1EV_IL2. These findings indicate that M1EV_IL2 promoted $CD8^+$ T cell activation and proliferation, highlighting its potential to enhance antitumor immunity within the TME.

To assess the $CD8^+$ T cell activation, qRT-PCR was performed to analyze the expression levels of representative activation markers, including granzyme B, IFN-γ, and tumor necrosis factor-alpha (TNF-α) (Figure 5G–H). The granzyme B expression level was only increased by 1.6 ± 0.8-fold in the M1EV group compared to that in the CTRL group, whereas a 464.4 ± 77.0-fold increase was observed in the M1EV_IL2 group. This level was comparable to the 473.1 ± 65.7-fold increase in the IL-2 group, suggesting that M1EV_IL2 activated $CD8^+$ T cells that can further induce cytotoxic responses. Similarly, the gene expression level of IFN-γ, another representative activation marker, was increased by 2.4 ± 1.5-fold in the M1EV group and by 129.5 ± 31.1-fold in the M1EV_IL2 group compared to that in the CTRL group. No significant difference was observed between the M1EV and CTRL groups, and the level in the M1EV_IL2 group was comparable to that in the IL-2 group, which exhibited a 152.3 ± 45.8-fold increase. The expression level of the pro-inflammatory cytokine TNF-α further confirmed that M1EV_IL2 successfully activated naïve $CD8^+$ T cells. Compared to that in the CTRL group, TNF-α expression was elevated by 11.6 ± 1.5-fold by M1EV_IL2, and the activation was evident based on the relative difference in gene expression compared to that in both the CTRL and M1EV groups. Consequently, $CD8^+$ T cells were successfully activated via IL-2 displayed on the surface of M1EV, leading to their proliferation and the secretion of key cytokines associated with adaptive immune responses. Furthermore, 10 μL of M1EV or M1EV_IL2 at a concentration of approximately 1.6×10^{11} particles/mL was administered to naïve $CD8^+$ T cells. Based on this, the concentration of IL-2 in M1EV_IL2 as analyzed by ELISA (Figure 3I) was calculated and found to be approximately 25-fold lower than that of the free IL-2 group. Despite this, comparable immunostimulatory effects were observed. This may be due to the biocompatible and cell-to-cell communicative properties of EVs, which enhance the delivery efficiency of IL-2 by maintaining its stability.[69–71] These findings are expected to have a positive impact on future in vivo and clinical studies. This suggests that IL-2 displayed to the M1EV surface exerted enhanced functional activity compared to free IL-2 and may serve as a more effective strategy to activate exhausted or naïve $CD8^+$ T cells and promote the proliferation of activated T cells within the TME.

Conclusion

Cancer remains a global public health challenge, and there are still many obstacles to overcome. Despite promising therapeutic strategies such as CAR-T cell therapy, significant limitations remain in effectively modulating the TME.[72] To overcome this, research on engineering immunotherapies based on nanomaterials is continuously being.[72,73] In this context, we developed a multifunctional cancer immunotherapeutic, M1EV_IL2. M1EV_IL2 effectively induced the repolarization of M2 macrophages to M1 macrophages. Simultaneously, M1EV_IL2 successfully promoted $CD4^+$ T cell activation. Furthermore, ex vivo experiments using naïve $CD8^+$ T cells isolated from mouse spleen demonstrated the naïve $CD8^+$ T cell activation to effector $CD8^+$ T cells by M1EV_IL2, validating the M1EV_IL2 T cell activation effect. Therefore, M1EV_IL2, with the unique functionality of M1EV, repolarizes M2 macrophages to M1 macrophages within the TME, creating a pro-inflammatory environment that suppresses cancer. Additionally, by activating naïve or exhausted T cells through the IL-2 displayed on its surface, M1EV_IL2 facilitates direct tumor attack, contributing to the improvement of the immune environment within the TME. M1EV_IL2 exhibits distinct advantages over conventional cancer treatment strategies. These findings suggest that M1EV_IL2 holds promise as a multifunctional cancer immunotherapeutic agent. Furthermore, M1EV_IL2, unlike previous studies, harnesses the unique characteristics of EVs and, through the synergy with the IL-2 displayed on its surface, demonstrates novelty as a dual immune-regulating multifunctional therapeutic that simultaneously modulates both innate and adaptive immunity. To clearly evaluate the antitumor effects, evaluation of the in vivo efficacy of M1EV_IL2 within the TME is essential. Thus, the therapeutic effects will be compared with those of conventional immunotherapies, such as IL-2 and immune checkpoint inhibitors

like anti-PD-L1, to assess the superior functionality of M1EV_IL2 and further explore its clinical potential. Furthermore, it will be essential to perform repeated stimulation experiments assessing T-cell persistence, potential exhaustion or activation-induced cell death, and to monitor Treg activation and expansion. Additional evaluation of M1EV_IL2 stability under harsh conditions will also be essential for future clinical translation and formulation development. Unlike other immunotherapeutic approaches, M1EV_IL2 possesses the following advantages. Firstly, by enhancing immune responses rather than directly targeting cancer cells, our approach may reduce the risk of adverse effects. Secondly, by stimulating innate and adaptive immune responses, M1EV_IL2 can maximize immune synergy, modulate the TME, and ultimately enhance therapeutic efficacy.

Acknowledgments

This work was supported by a National Research Foundation of Korea (NRF) Grant funded by the Korean government (MSIT) (RS-2022-NR069930). This work was supported by the Incheon National University Research Grant in 2022.

Disclosure

The authors report no conflicts of interest in this work.

References

1. Siegel RL, Giaquinto AN, Jemal A. Cancer statistics, 2024. *Ca A Cancer J Clinicians*. 2024;74(1):12–49. doi:10.3322/caac.21820
2. Bray F, Laversanne M, Sung H, et al. Global cancer statistics 2022: GLOBOCAN estimates of incidence and mortality worldwide for 36 cancers in 185 countries. *Ca A Cancer J Clinicians*. 2024;74(3):229–263. doi:10.3322/caac.21834
3. Yang M, Olaoba OT, Zhang C, Kimchi ET, Staveley-O'Carroll KF, Li G. Cancer immunotherapy and delivery system: an update. *Pharmaceutics*. 2022;14(8):1630. doi:10.3390/pharmaceutics14081630
4. Choi Y, Lee JH, Kim YH, et al. Impact of postthyroidectomy scar on the quality of life of thyroid cancer patients. *Ann Dermatol*. 2014;26(6):693–699. doi:10.5021/ad.2014.26.6.693
5. Sui X, Chen R, Wang Z, et al. Autophagy and chemotherapy resistance: a promising therapeutic target for cancer treatment. *Cell Death Dis*. 2013;4(10):e838. doi:10.1038/cddis.2013.350
6. van den Boogaard WMC, Komninos DSJ, Vermeij WP. Chemotherapy side-effects: not all DNA damage is equal. *Cancers*. 2022;14(3):627. doi:10.3390/cancers14030627
7. Riley RS, June CH, Langer R, Mitchell MJ. Delivery technologies for cancer immunotherapy. *Nat Rev Drug Discov*. 2019;18(3):175–196. doi:10.1038/s41573-018-0006-z
8. Liu C, Yang M, Zhang D, Chen M, Zhu D. Clinical cancer immunotherapy: current progress and prospects. *Front Immunol*. 2022;13:961805. doi:10.3389/fimmu.2022.961805
9. Marcus L, Fashoyin-Aje LA, Donoghue M, et al. FDA approval summary: pembrolizumab for the treatment of tumor mutational burden-high solid tumors. *Clin Cancer Res*. 2021;27(17):4685–4689. doi:10.1158/1078-0432.CCR-21-0327
10. Kubli SP, Berger T, Araujo DV, Siu LL, Mak TW. Beyond immune checkpoint blockade: emerging immunological strategies. *Nat Rev Drug Discov*. 2021;20(12):899–919. doi:10.1038/s41573-021-00155-y
11. Zhang W, Hu X, Cheng W, et al. Harnessing nanomaterials to precisely regulate the immunosuppressive tumor microenvironment for enhanced immunotherapy. *BMEMat*;2025. 70019. doi:10.1002/bmm2.70019
12. Xiao Y, Yu D. Tumor microenvironment as a therapeutic target in cancer. *Pharmacol Ther*. 2021;221:107753. doi:10.1016/j.pharmthera.2020.107753
13. Senovilla L, Vacchelli E, Galon J, et al. Trial watch: prognostic and predictive value of the immune infiltrate in cancer. *Oncoimmunology*. 2012;1(8):1323–1343. doi:10.4161/onci.22009
14. Qian BZ, Pollard JW. Macrophage diversity enhances tumor progression and metastasis. *Cell*. 2010;141(1):39–51. doi:10.1016/j.cell.2010.03.014
15. Chanmee T, Ontong P, Konno K, Itano N. Tumor-associated macrophages as major players in the tumor microenvironment. *Cancers*. 2014;6(3):1670–1690. doi:10.3390/cancers6031670
16. Cassetta L, Pollard JW. Targeting macrophages: therapeutic approaches in cancer. *Nat Rev Drug Discov*. 2018;17(12):887–904. doi:10.1038/nrd.2018.169
17. Basak U, Sarkar T, Mukherjee S, et al. Tumor-associated macrophages: an effective player of the tumor microenvironment. *Front Immunol*. 2023;14:1295257. doi:10.3389/fimmu.2023.1295257
18. Fridman WH, Pagès F, Sautès-Fridman C, Galon J. The immune contexture in human tumours: impact on clinical outcome. *Nat Rev Cancer*. 2012;12(4):298–306. doi:10.1038/nrc3245
19. Friedman KM, Prieto PA, Devillier LE, et al. Tumor-specific CD4+ melanoma tumor-infiltrating lymphocytes. *J Immunotherap*. 2012;35(5):400–408. doi:10.1097/CJI.0b013e31825898c5
20. Hadrup S, Donia M, Thor Straten P. Effector CD4 and CD8 T cells and their role in the tumor microenvironment. *Cancer Microenvironment*. 2013;6(2):123–133. doi:10.1007/s12307-012-0127-6
21. Anderson NM, Simon MC. The tumor microenvironment. *Current Biology*. 2020;30(16):R921–r925. doi:10.1016/j.cub.2020.06.081
22. Jiang Y, Li Y, Zhu B. T-cell exhaustion in the tumor microenvironment. *Cell Death Dis*. 2015;6(6):e1792. doi:10.1038/cddis.2015.162
23. Heintzman DR, Fisher EL, Rathmell JC. Microenvironmental influences on T cell immunity in cancer and inflammation. *Cell Mol Immunol*. 2022;19(3):316–326. doi:10.1038/s41423-021-00833-2

24. Colombo M, Raposo G, Théry C. Biogenesis, secretion, and intercellular interactions of exosomes and other extracellular vesicles. *Annu Rev Cell Dev Biol*. 2014;30(1):255–289. doi:10.1146/annurev-cellbio-101512-122326
25. Tkach M, Théry C. Communication by extracellular vesicles: where we are and where we need to go. *Cell*. 2016;164(6):1226–1232. doi:10.1016/j.cell.2016.01.043
26. van Niel G, D'Angelo G, Raposo G. Shedding light on the cell biology of extracellular vesicles. *Nat Rev Mol Cell Biol*. 2018;19(4):213–228. doi:10.1038/nrm.2017.125
27. Veerman RE, Teeuwen L, Czarnewski P, et al. Molecular evaluation of five different isolation methods for extracellular vesicles reveals different clinical applicability and subcellular origin. *J Extracell Vesicles*. 2021;10(9):e12128. doi:10.1002/jev2.12128
28. Valadi H, Ekström K, Bossios A, Sjöstrand M, Lee JJ, Lötvall JO. Exosome-mediated transfer of mRNAs and microRNAs is a novel mechanism of genetic exchange between cells. *Nat Cell Biol*. 2007;9(6):654–659. doi:10.1038/ncb1596
29. Tian T, Wang Y, Wang H, Zhu Z, Xiao Z. Visualizing of the cellular uptake and intracellular trafficking of exosomes by live-cell microscopy. *J Cell Biochem*. 2010;111(2):488–496. doi:10.1002/jcb.22733
30. Kim H, Park HJ, Chang HW, et al. Exosome-guided direct reprogramming of tumor-associated macrophages from protumorigenic to antitumorigenic to fight cancer. *Bioact Mater*. 2023;25:527–540. doi:10.1016/j.bioactmat.2022.07.021
31. Gunassekaran GR, Poongkavithai Vadevoo SM, Baek MC, Lee B. M1 macrophage exosomes engineered to foster M1 polarization and target the IL-4 receptor inhibit tumor growth by reprogramming tumor-associated macrophages into M1-like macrophages. *Biomaterials*. 2021;278:121137. doi:10.1016/j.biomaterials.2021.121137
32. Wang S, Shi Y. Exosomes derived from immune cells: the new role of tumor immune microenvironment and tumor therapy. *Int J Nanomed*. 2022;17:6527–6550. doi:10.2147/IJN.S388604
33. Li G, Chen T, Dahlman J, et al. Current challenges and future directions for engineering extracellular vesicles for heart, lung, blood and sleep diseases. *J Extracell Vesicles*. 2023;12(2):e12305. doi:10.1002/jev2.12305
34. Richter M, Vader P, Fuhrmann G. Approaches to surface engineering of extracellular vesicles. *Adv Drug Delivery Rev*. 2021;173:416–426. doi:10.1016/j.addr.2021.03.020
35. Cheng Q, Dai Z, Smbatyan G, Epstein AL, Lenz HJ, Zhang Y. Eliciting anti-cancer immunity by genetically engineered multifunctional exosomes. *Molecular Therap*. 2022;30(9):3066–3077. doi:10.1016/j.ymthe.2022.06.013
36. Li P, Xie Y, Wang J, et al. Gene engineered exosome reverses T cell exhaustion in cancer immunotherapy. *Bioact Mater*. 2024;34:466–481. doi:10.1016/j.bioactmat.2024.01.008
37. Yang Y, Xiu F, Cai Z, et al. Increased induction of antitumor response by exosomes derived from interleukin-2 gene-modified tumor cells. *J Cancer Res Clin Oncol*. 2007;133(6):389–399. doi:10.1007/s00432-006-0184-7
38. Jung D, Shin S, Kang SM, et al. Reprogramming of T cell-derived small extracellular vesicles using IL2 surface engineering induces potent anti-cancer effects through miRNA delivery. *J Extracell Vesicles*. 2022;11(12):e12287. doi:10.1002/jev2.12287
39. Mahmoudi M, Taghavi-Farahabadi M, Hashemi SM, Mousavizadeh K, Rezaei N, Mojtabavi N. Reprogramming tumor-associated macrophages using exosomes from M1 macrophages. *Biochem Biophys Res Commun*. 2024;733:150697. doi:10.1016/j.bbrc.2024.150697
40. Moradi-Chaleshtori M, Bandehpour M, Heidari N, Mohammadi-Yeganeh S, Mahmoud Hashemi S. Exosome-mediated miR-33 transfer induces M1 polarization in mouse macrophages and exerts antitumor effect in 4T1 breast cancer cell line. *Int Immunopharmacol*. 2021;90:107198. doi:10.1016/j.intimp.2020.107198
41. Moradi-Chaleshtori M, Bandehpour M, Soudi S, Mohammadi-Yeganeh S, Hashemi SM. In vitro and in vivo evaluation of anti-tumoral effect of M1 phenotype induction in macrophages by miR-130 and miR-33 containing exosomes. *Cancer Immunol Immunotherap*. 2021;70(5):1323–1339. doi:10.1007/s00262-020-02762-x
42. Lyu C, Sun H, Sun Z, Liu Y, Wang Q. Roles of exosomes in immunotherapy for solid cancers. *Cell Death Dis*. 2024;15(2):106. doi:10.1038/s41419-024-06494-z
43. Agatemor C, Buettner MJ, Ariss R, Muthiah K, Saeui CT, Yarema KJ. Exploiting metabolic glycoengineering to advance healthcare. *Nature Rev Chem*. 2019;3(10):605–620. doi:10.1038/s41570-019-0126-y
44. Kufleitner M, Haiber LM, Wittmann V. Metabolic glycoengineering - exploring glycosylation with bioorthogonal chemistry. *Chem Soc Rev*. 2023;52(2):510–535. doi:10.1039/D2CS00764A
45. Boyce M, Bertozzi CR. Bringing chemistry to life. *Nature Methods*. 2011;8(8):638–642. doi:10.1038/nmeth.1657
46. Smyth T, Petrova K, Payton NM, et al. Surface functionalization of exosomes using click chemistry. *Bioconjugate Chem*. 2014;25(10):1777–1784. doi:10.1021/bc500291r
47. Ruan H, Li Y, Wang C, et al. Click chemistry extracellular vesicle/peptide/chemokine nanocarriers for treating central nervous system injuries. *Acta Pharmaceutica Sinica B*. 2023;13(5):2202–2218. doi:10.1016/j.apsb.2022.06.007
48. Yoon HI, Yhee JY, Na JH, et al. Bioorthogonal copper free click chemistry for labeling and tracking of chondrocytes in vivo. *Bioconjugate Chem*. 2016;27(4):927–936. doi:10.1021/acs.bioconjchem.6b00010
49. Yunna C, Mengru H, Lei W, Weidong C. Macrophage M1/M2 polarization. *Eur J Pharmacol*. 2020;877:173090. doi:10.1016/j.ejphar.2020.173090
50. Daigneault M, Preston JA, Marriott HM, Whyte MK, Dockrell DH. The identification of markers of macrophage differentiation in PMA-stimulated THP-1 cells and monocyte-derived macrophages. *PLoS One*. 2010;5(1):e8668. doi:10.1371/journal.pone.0008668
51. Li P, Hao Z, Wu J, et al. Comparative proteomic analysis of polarized human THP-1 and mouse RAW264.7 macrophages. *Front Immunol*. 2021;12:700009. doi:10.3389/fimmu.2021.700009
52. Kalluri R, LeBleu VS. The biology, function, and biomedical applications of exosomes. *Science*. 2020;367(6478). doi:10.1126/science.aau6977
53. Jorquera-Cordero C, Lara P, Cruz LJ, et al. Extracellular vesicles from M1-polarized macrophages combined with hyaluronic acid and a β-blocker potentiate doxorubicin's antitumor activity by downregulating tumor-associated macrophages in breast cancer. *Pharmaceutics*. 2022;14(5):1068. doi:10.3390/pharmaceutics14051068
54. Cheng L, Wang Y, Huang L. Exosomes from M1-polarized macrophages potentiate the cancer vaccine by creating a pro-inflammatory microenvironment in the lymph node. *Molecular Therap*. 2017;25(7):1665–1675. doi:10.1016/j.ymthe.2017.02.007
55. Zhao Q, Kim T, Pang J, et al. A novel function of CXCL10 in mediating monocyte production of proinflammatory cytokines. *J Leukocyte Biol*. 2017;102(5):1271–1280. doi:10.1189/jlb.5A0717-302

56. Xu ZJ, Gu Y, Wang CZ, et al. The M2 macrophage marker CD206: a novel prognostic indicator for acute myeloid leukemia. *Oncoimmunology*. 2020;9(1):1683347. doi:10.1080/2162402X.2019.1683347
57. Iwasaki A, Medzhitov R. Regulation of adaptive immunity by the innate immune system. *Science*. 2010;327(5963):291–295. doi:10.1126/science.1183021
58. Hinrichs CS, Spolski R, Paulos CM, et al. IL-2 and IL-21 confer opposing differentiation programs to CD8+ T cells for adoptive immunotherapy. *Blood*. 2008;111(11):5326–5333. doi:10.1182/blood-2007-09-113050
59. Boyman O, Sprent J. The role of interleukin-2 during homeostasis and activation of the immune system. *Nat Rev Immunol*. 2012;12(3):180–190. doi:10.1038/nri3156
60. Pipkin ME, Sacks JA, Cruz-Guilloty F, Lichtenheld MG, Bevan MJ, Rao A. Interleukin-2 and inflammation induce distinct transcriptional programs that promote the differentiation of effector cytolytic T cells. *Immunity*. 2010;32(1):79–90. doi:10.1016/j.immuni.2009.11.012
61. Borst J, Ahrends T, Bąbała N, Melief CJM, Kastenmüller W. CD4(+) T cell help in cancer immunology and immunotherapy. *Nat Rev Immunol*. 2018;18(10):635–647. doi:10.1038/s41577-018-0044-0
62. Constant SL, Bottomly K. INDUCTION OF TH1 AND TH2 CD4 + T CELL RESPONSES:The Alternative Approaches. *Ann Rev Immunol*. 1997;15(1):297–322. doi:10.1146/annurev.immunol.15.1.297
63. Shatrova AN, Mityushova EV, Aksenov NA, Marakhova II. CD25 expression on the surface of Jurkat cells. *Cell Tissue Biol*. 2015;9(5):364–370. doi:10.1134/S1990519X15050119
64. Miyajima C, Itoh Y, Inoue Y, Hayashi H. Positive regulation of interleukin-2 expression by a pseudokinase, tribbles 1, in activated T cells. *Biol Pharm Bull*. 2015;38(8):1126–1133. doi:10.1248/bpb.b15-00002
65. Wang X, Wang J, Liang C, Xu S. IL-2 and IFN-γ secretion of activated jurkat T cells via a Microdroplet-SERS based single-cell immunoassay (Drop-SCIA). *Anal Chem*. 2025;97(33):18064–18074. doi:10.1021/acs.analchem.5c02142
66. Philip M, Schietinger A. CD8(+) T cell differentiation and dysfunction in cancer. *Nat Rev Immunol*. 2022;22(4):209–223. doi:10.1038/s41577-021-00574-3
67. Cao X, Cai SF, Fehniger TA, et al. Granzyme B and perforin are important for regulatory T cell-mediated suppression of tumor clearance. *Immunity*. 2007;27(4):635–646. doi:10.1016/j.immuni.2007.08.014
68. Smith GA, Taunton J, Weiss A. IL-2Rβ abundance differentially tunes IL-2 signaling dynamics in CD4(+) and CD8(+) T cells. *Sci Signaling*. 2017;10(510). doi:10.1126/scisignal.aan4931
69. Kamerkar S, LeBleu VS, Sugimoto H, et al. Exosomes facilitate therapeutic targeting of oncogenic KRAS in pancreatic cancer. *Nature*. 2017;546(7659):498–503. doi:10.1038/nature22341
70. Kim KM, Abdelmohsen K, Mustapic M, Kapogiannis D, Gorospe M. RNA in extracellular vesicles. *WIREs RNA*. 2017;8(4):e1413. doi:10.1002/wrna.1413
71. Balaj L, Lessard R, Dai L, et al. Tumour microvesicles contain retrotransposon elements and amplified oncogene sequences. *Nat Commun*. 2011;2(1):180. doi:10.1038/ncomms1180
72. Chen K, Wang W, Wang Z. Designing next-generation immune cell therapies with nanomaterials. *BMEMat*. 2025;3(2):e70003. doi:10.1002/bmm2.70003
73. Shen J, Zhou Y, Yin L. Nano/genetically engineered cells for immunotherapy. *BMEMat*. 2025;3(1):e12112. doi:10.1002/bmm2.12112